Hindawi Publishing Corporation
EURASIP Journal on Wireless Communications and Networking
Volume 2010, Article ID 143413, 12 pages
doi:10.1155/2010/143413

Research Article

Dynamic Resource Partitioning for Downlink Femto-to-Macro-Cell Interference Avoidance

Zubin Bharucha,[1] Andreas Saul,[1] Gunther Auer,[1] and Harald Haas[2]

[1] *DOCOMO Communications Laboratories Europe GmbH, Landsberger Straße 312, 80687 Munich, Germany*
[2] *School of Engineering and Electronics, Institute for Digital Communications, Joint Research Institute for Signal and Image Processing, The University of Edinburgh, Edinburgh EH9 3JL, UK*

Correspondence should be addressed to Zubin Bharucha, bharucha@docomolab-euro.com

Received 31 December 2009; Accepted 26 April 2010

Academic Editor: Holger Claussen

Femto-cells consist of user-deployed Home Evolved NodeBs (HeNBs) that promise substantial gains in system spectral efficiency, coverage, and data rates due to an enhanced reuse of radio resources. However, reusing radio resources in an uncoordinated, random fashion introduces potentially destructive interference to the system, both, in the femto and macro layers. An especially critical scenario is a closed-access femto-cell, cochannel deployed with a macro-cell, which imposes strong downlink interference to nearby macro user equipments (UEs) that are not permitted to hand over to the femto-cell. In order to maintain reliable service of macro-cells, it is imperative to mitigate the destructive femto-cell to macro-cell interference. The contribution in this paper focuses on mitigating downlink femto-cell to macro-cell interference through dynamic resource partitioning, in the way that HeNBs are denied access to downlink resources that are assigned to macro UEs in their vicinity. By doing so, interference to the most vulnerable macro UEs is effectively controlled at the expense of a modest degradation in femto-cell capacity. The necessary signaling is conveyed through downlink high interference indicator (DL-HII) messages over the wired backbone. Extensive system level simulations demonstrate that by using resource partitioning, for a sacrifice of 4% of overall femto downlink capacity, macro UEs exposed to high HeNB interference experience a tenfold boost in capacity.

1. Introduction

There is a growing demand for increased user and system throughput in wireless networks. Naturally, such rapidly increasing demand is served by higher bandwidth allocation, but because bandwidth is scarce and expensive, a key to substantial throughput enhancement is to increase the spatial reuse of radio frequency resources. One powerful method of boosting wireless capacity is by shrinking the cell size. The reason for this is that smaller cell sizes enable a more efficient spatial reuse of spectrum [1]. Furthermore, the shorter transmission distances enhance link capacity due to higher channel gains [2].

Studies indicate that a significant proportion of data traffic originates indoors [3]. Poor signal reception caused by penetration losses through walls severely hampers the operation of indoor data services in state-of-the-art systems. Recently, the concept of 3rd generation (3G) and beyond 3G (B3G) femto-cells, in which HeNBs are placed indoors, has therefore attracted considerable interest. HeNBs are low-cost, low-power, short-range, plug-and-play base stations that are directly connected to the backbone network. HeNBs aim at extending broadband coverage to authorized UEs located indoors where it is most needed [3]. HeNBs therefore offload indoor users from the macro-cell, thus potentially enhancing the capacity both indoors by bypassing wall penetration losses, as well as outdoors by freeing up resources [4, 5]. Moreover, femto-cell deployment could potentially lead to an overall reduced energy consumption as penetration losses due to walls are circumvented [6].

In [7–9], the authors propose the *TDD underlay* concept. Owing to the asymmetric nature of traffic [10], one of the frequency division duplex (FDD) bands (the underloaded one) can be split in time such that the HeNB transmits and

receives information from its associated UE in a time division duplex (TDD) fashion. This proposal, while making efficient utilization of unused resources, still encounters a bottleneck, because typically, the link between the HeNB and its femto UEs is much stronger than that between the evolved NodeB (eNB) and the macro UE.

In this paper, both macro and femto-cells are assumed to operate in the same radio frequency spectrum in FDD mode, compliant with the specifications for B3G mobile communication systems [11]. Like in the original TDD underlay concept [7], the HeNB backhauls data through a dedicated broadband gateway (DSL/Ethernet/etc.) to the cellular operator network.

However, HeNBs are deployed without network planning, such that their deployment introduces additional interference [12]. Regarding hand-over between macro and femto-cells, two access control mechanisms, *open-access* and *closed-access*, are identified. In open-access femto-cells, macro UEs get *assimilated* into the femto-cell, which means that UEs that lie within the coverage area of a femto-cell are handed over to the corresponding HeNB. In closed-access systems the HeNB only grants access to a particular set of authorized UEs. It is these closed-access systems that cause (and receive) the most detrimental interference. This is because a "foreign" macro UE lying in the coverage area of a femto-cell is not allowed to communicate with the HeNB, but must communicate with the eNB that lies outdoors. Due to wall penetration losses, such macro UEs receive a highly attenuated signal from the eNB and, in addition, receive excessive interference originating from the HeNBs in whose coverage areas the macro UE lies. No matter the access control, it is crucial that the provision of base-coverage by the macro-cell network is not compromised by femto-cell deployment.

In [13], the feasibility of the coexistence of cochannel macro and femto-cells has been investigated. A power control method is defined in the downlink such that a constant femto-cell radius is maintained. In [14], the authors analyze the impact of femto-cell deployment on the macro-cell performance. In all of these papers, no active interference avoidance technique is discussed. In [15], the authors analyze the uplink capacity and interference avoidance for networks consisting of macro and femto-cells existing together in a code division multiple access (CDMA) network. In particular, the authors evaluate a network-wide area spectral efficiency metric, that is defined as the feasible combinations of the average number of macro-cell UEs and HeNBs per eNB that satisfy a target outage constraint. Interference avoidance in this case is done via a time-hopped CDMA physical layer and sectorization of antennas. In contrast to the above, the contribution in this paper comes in the form of a novel dynamic downlink interference avoidance technique that prioritizes macro UEs for a spectrum sharing orthogonal frequency division multiple access (OFDMA) system. The reason for this is twofold. First, the downlink is more critical in terms of femto-to-macro interference, because it is more likely that a macro UE suffers from downlink interference from a nearby HeNB than an eNB suffers from uplink interference from a femto UE, due to the asymmetry in cell-size, and the corresponding asymmetry in transmit powers, between macro and femto-cells. Second, priority should generally be given to the macro layer rather than the femto layer. To this end, if an HeNB is perceived to interfere severely with a macro UE, it must act so as to nullify this interference by smartly scheduling (partitioning) its resources. If no macro UE is affected, the femto-cell may use all resources (full frequency reuse).

For the B3G mobile communication system 3rd generation partnership project (3GPP) Long-Term Evolution (LTE) [11], high interference indicator (HII) messages are specified to deal with macro-to-macro interference in the uplink [16, 17], that are conveyed through the X2 interface via the wired backbone. In this work, it is demonstrated that the same framework can be applied for downlink interference coordination between macro and femto-cells, by signaling downlink high interference indicator (DL-HII) messages via an X2 connection to femto-cells.

In order to assess the impact of resource partitioning on macro and femto-cell performance, system level simulations are carried out. The performance of a closed-access system is compared against the performance of the same distribution of users using the aforementioned resource partitioning scheme. For comparison purposes, a benchmark system is simulated that closely reflects state-of-the-art cellular networks in which there are no HeNBs, and all femto UEs are served by eNBs.

2. System and Channel Model

The downlink of an OFDMA system is considered, where the system bandwidth B is divided into N resource blocks (RBs), $B = NB_{\mathrm{RB}}$. An RB represents one basic time-frequency unit with bandwidth B_{RB}. All eNBs transmit with a fixed power per RB, P_{m}, and all HeNBs transmit with a fixed power, P_{f}, per RB. Perfect synchronization in time and frequency is assumed.

Universal frequency reuse is considered, so that both macro and femto-cells utilize the entire system bandwidth B. Multiple receive antennas are assumed, and the M received signal streams are combined with maximum ratio combining (MRC). The gain from MRC is approximated by simulating M individual, uncorrelated receive streams and adding the achieved signal-to-interference-plus-noise ratio (SINR) [18]. The set of available RBs $\mathcal{N}$, with cardinality $|\mathcal{N}| = N$, is distributed by eNBs and HeNBs among their associated macro and femto UEs, respectively. Throughout this paper, u is used to identify any macro or femto UE, and v_u denotes the H/eNB that serves UE u. The received signal power observed by UE u at RB n is given by

$$Y_n^u = P_u \sum_m^M G_{m,n}^{u,v_u} + I_n^u + \eta, \tag{1}$$

where $G_{m,n}^{u,v_u}$ is the channel gain between UE u and its serving HeNB or eNB v_u, observed at receive antenna m and at RB n. Furthermore, η accounts for thermal noise per RB, which is constant across all RBs. The transmit power is set to $P_u = P_{\mathrm{m}}$, and $P_u = P_{\mathrm{f}}$ if UE u is served by an eNB or HeNB,

Table 1: Link to system mapping parameters.

Parameter	Value	Notes
α	0.6	Implementation losses
$\gamma_{\min}$ [dB]	−10	QPSK
$\gamma_{\max}$ [dB]	19.5	64QAM
$\overline{C}_{\max}$ [bps/Hz]	4.4	64QAM

respectively. The aggregate interference I_n^u is composed of macro and femto-cell interference

$$I_n^u = \sum_m^M \left\{ \sum_{i \in \mathcal{M}_{\text{int}}} G_{m,n}^{u,i} P_{\text{m}} + \sum_{i \in \mathcal{F}_{\text{int}}} G_{m,n}^{u,i} P_{\text{f}} \right\}, \tag{2}$$

where the first and second addends represent the macro and femto-cell interference, respectively. The set of interfering eNBs and HeNBs are denoted by $\mathcal{M}_{\text{int}}$ and $\mathcal{F}_{\text{int}}$. In case UE u is served by an eNB v_u, $\mathcal{M}_{\text{int}}$ comprises all eNBs except for v_u, that is, $v_u \notin \mathcal{M}_{\text{int}}$. In this case, $\mathcal{F}_{\text{int}}$ is the set of all HeNBs in the system. Likewise, if UE_u is served by an HeNB v_u, then $v_u \notin \mathcal{F}_{\text{int}}$. The SINR observed by UE u at RB n amounts to

$$\gamma_n^u = \frac{P_u \sum_m^M G_{m,n}^{u,v_u}}{I_n^u + \eta}. \tag{3}$$

Due to MRC at the receiver, the channel gains $G_{m,n}^{u,v_u}$ add constructively, so that the average SINR is increased by a factor of M, together with an M-fold diversity gain.

Link adaptation is implemented where the modulation and coding scheme used are selected based on the achieved SINR. In order to model link adaptation, the SINR is mapped to the capacity using the *attenuated and truncated Shannon bound* method [19]. Given a particular SINR γ_n^u, the spectral efficiency on RB n for UE u, $\overline{C}_n^u$, is determined by

$$\overline{C}_n^u = \begin{cases} 0 & \text{for } \gamma_n^u < \gamma_{\min}, \\ \alpha S(\gamma_n^u) & \text{for } \gamma_{\min} < \gamma_n^u < \gamma_{\max}, \\ \overline{C}_{\max} & \text{for } \gamma_n^u > \gamma_{\max}, \end{cases} \tag{4}$$

where $S(x) = \log_2(1+x)$ in [bit/s/Hz] is the Shannon bound, α is the attenuation factor representing implementation losses, and $\gamma_{\min}$ and $\gamma_{\max}$ are the minimum and maximum SINRs supported by the available modulation and coding schemes. These parameters are summarized in Table 1. The capacity C_u of UE_u is then calculated as the aggregate capacity on all the RBs allocated to it as

$$C_u = B_{\text{RB}} \sum_{i \in \mathcal{N}_u} \overline{C}_i^u, \tag{5}$$

where $\mathcal{N}_u$ is the set of RBs allocated to user u. The value for $\gamma_{\max}$ is taken from [20] based on a maximum modulation scheme of 64-QAM in the downlink.

2.1. Channel Model. The channel gain, $G_{m,n}^{u,v}$, between a transmitter v and a receiver u, observed at receive antenna m on RB n as defined in (1) is composed of distance-dependent path loss, log-normal shadowing, and channel variations due to frequency-selective fading:

$$G_{m,n}^{u,v} = \left| H_{m,n}^{u,v} \right|^2 10^{(-L(d)+X_\sigma)/10}, \tag{6}$$

where $H_{m,n}^{u,v}$ accounts for the channel transfer factor between transmitter v and receiver u observed at receive antenna m at RB n, $L(d)$ is the distance-dependent path loss (in dB), and X_σ is the log-normal shadowing value (in dB) with standard deviation σ [21]. Channel variations of $H_{m,n}^{u,v}$ on different receive antennas are mutually independent, while the path loss $L(d)$ is identical for all receive antennas m and RBs n. While the channel response generally exhibits time and frequency dispersions, channel fluctuations within an RB are neglected because the RB dimensions are significantly smaller than the coherence time and coherence frequency of the channel [22]. The delay profiles associated with applicable propagation scenarios of [21, 23] are used to generate the frequency-selective fading channel transfer factor $H_{m,n}^{u,v}$.

Table 2: Shadowing parameters.

	Macro-cell	Femto-cell
Standard Deviation, σ	8 dB	10 dB
Auto-correlation distance	50 m	3 m

2.2. Path Loss Models. Three path loss models are used depending on the type of link, as prescribed in [24]. For a purely outdoor link, that is, the link (useful or interfering) between an eNB and an outdoor macro UE, the path loss is calculated as

$$L\,[\text{dB}] = 15.3 + 37.6 \log_{10}(R), \tag{7}$$

where R (in m) is the distance between the transmitter and the receiver.

When considering the useful/interfering link between an eNB and a macro UE situated indoors or the interfering link between a femto UE (which is always situated indoors) and an eNB, the path loss includes the wall penetration loss and is calculated as

$$L\,[\text{dB}] = 15.3 + 37.6 \log_{10}(R) + L_{\text{W}}, \tag{8}$$

where L_{W} is the wall penetration loss (in dB).

Finally, when considering the useful/interfering link between an HeNB and a femto UE or the interfering link between a macro UE and an HeNB, the path loss is calculated as

$$L\,[\text{dB}] = 127 + 30 \log_{10}\left(\frac{R}{1000}\right). \tag{9}$$

This is a simplified model based on LTE-A evaluation methodology that avoids modelling any walls.

Log-normal shadowing is added to all links. Correlated shadowing maps are applied such that the correlation in

the shadowing values of two points is dependent on the distance between them. Table 2 shows the shadowing standard deviation σ and auto-correlation shadowing distances for the macro and femto-cells [24].

3. Femto-Cell Resource Partitioning

3.1. Downlink Interference Scenario for Closed-Access. As the eNB transmit power typically exceeds the HeNB transmit power by several orders of magnitude, $P_{\mathrm{f}} \ll P_{\mathrm{m}}$, in most cases, the interference seen by macro UE u will be dominated by eNB interference. Only if a macro-cell receiver, UE u, is located in close proximity to an HeNB i, UE u is exposed to high HeNB interference $G_n^{u,i}P_{\mathrm{f}}$, $i \in \mathcal{F}_{\mathrm{int}}$. In case UE u is located indoors, the situation is exacerbated by the poor channel gains, G_n^{u,v_u}, to the serving eNB v_u, caused by high wall penetration losses. This UE u is likely to experience poor SINR, (3). With full frequency reuse, femto-cells utilize all N RBs. Therefore, the received SINR is likely to be unacceptable over the entire set of RB allocated to UE u, that is, $\mathcal{N}_u$.

3.2. Avoiding Femto-to-Macro Interference. Suppose that macro UE u is located indoors within coverage of HeNB i, but served by an outdoor eNB v_u. An effective means of mitigating the destructive HeNB interference observed by UE u is to introduce the concept of resource partitioning, such that HeNB i is denied access to RBs, $\mathcal{N}_u$, that are assigned to UE u. In other words, the set of RBs allocated to UE u must be left idle by HeNB i. Doing so completely eliminates the interference originating from the interfering HeNB i, which, in this case, is the most dominant source of interference. This increases the SINR (3) achieved at the macro UE.

In order to implement femto-cell resource partitioning, a predefined interference threshold, I_{th}, is introduced. Each macro UE measures the average channel gains $\overline{G}^{u,v} = \mathrm{E}\{G_{m,n}^{u,v}\}$ of nearby HeNBs and performs the following threshold test:

$$10\log \mathrm{E}\left\{G_{m,n}^{u,v}\right\} = -L^{u,v}(d) + X_\sigma \geq I_{\mathrm{th}} - P_{\mathrm{f}} = G_{\mathrm{th}}. \quad (10)$$

In case the average channel gain between an HeNB and the vulnerable macro UEs exceeds G_{th}, the HeNB is instructed to perform resource partitioning by suppressing transmission on RBs that are reserved by the vulnerable macro UEs. Clearly, decreasing the value of I_{th} while keeping P_{f} fixed increases the size of the "exclusion region" and protects a larger number of macro UEs, as seen in Figure 2. Therefore, the lower the threshold I_{th}, the more resources are partitioned by HeNBs, so that the impact of resource partitioning on femto-cell performance increases as I_{th} decreases. The simulation results presented in Section 5 make use of two different values of I_{th} such that one translates to a large exclusion region and the other to a small one.

It is possible that more than one macro UE experiences heavy interference from more than one HeNB. Suppose that HeNB i causes strong interference to several UEs, as determined by the threshold test (10). Let the set of macro UEs exposed to strong interference from HeNB i be denoted by $\mathcal{U}_{\mathrm{aff}}^i$. The associated measurement and signaling procedures on how each UE in $\mathcal{U}_{\mathrm{aff}}^i$ identifies the interfering HeNB i are detailed in Section 3.3. As per the resource partitioning concept, HeNB i must partition resources such that it does not cause interference to the set of macro UEs $\mathcal{U}_{\mathrm{aff}}^i$. In other words, the resources that are prohibited for HeNB i are in the form

$$\overline{\mathcal{N}}_i = \bigcup_{u \in \mathcal{U}_{\mathrm{aff}}^i} \mathcal{N}_u \,. \quad (11)$$

We note that the affected macro UEs within $\mathcal{U}_{\mathrm{aff}}^i$ may be connected to different macro eNBs, as HeNB i may be within the coverage area of several macro-cells.

In general, every HeNB that causes high interference to nearby macro UEs must partition resources as explained by (11). However, due to the low HeNB transmit power, P_{f}, it is unlikely that *all* femto-cells cause high interference to many macro UEs. Hence, in most cases, only a small subset of the users served by an eNB are interfered by the same set of HeNBs, as illustrated in Figure 1. This implies that, in general, the number of RBs $|\overline{\mathcal{N}}_i| = \overline{N}_i$ that must not be used by an interfering HeNB is much smaller than the total number of RBs, $\overline{N}_i \ll N$, so that the overall degradation of femto-cell capacity is expected to be modest.

3.3. Practical Implementation in LTE Systems. In order to implement the resource partitioning concept, the interfering femto-cell needs to be identified and then be informed of the restricted resources $\overline{\mathcal{N}_i}$ it must not use according to (11). This involves integrating the proposed resource partitioning concept within the LTE network architecture. In abstract, femto-cell resource partitioning is integrated to the LTE network architecture by the following procedure.

(1) Macro UE u determines the cell-ID of surrounding HeNBs, by reading the corresponding broadcast channel (BCH), and stores them in a list containing neighboring cell-IDs.

(2) UE u identifies the heavily interfering HeNBs in its proximity using reference signal received power (RSRP) measurements.

(3) The cell-IDs of the corresponding HeNBs are reported to the serving eNB.

(4) The eNB prepares a DL-HII bitmap containing information about which RBs are transmitted with high power.

(5) The DL-HII bitmap is disseminated to neighboring H/eNBs over the X2 or S1 interfaces.

(6) If the receiving eNB is an HeNB, it will refrain from using the particular RBs marked in the DL-HII bitmap. In this way, detrimental downlink femto-cell interference at the vulnerable macro UEs is avoided.

The necessary UE measurements that identify which femto-cells are in close vicinity of a macro UE are similar to a handover procedure. In LTE, macro UEs read the broadcast channel (BCH) not only from their primary eNB, but also from one or several secondary eNBs. As the BCH

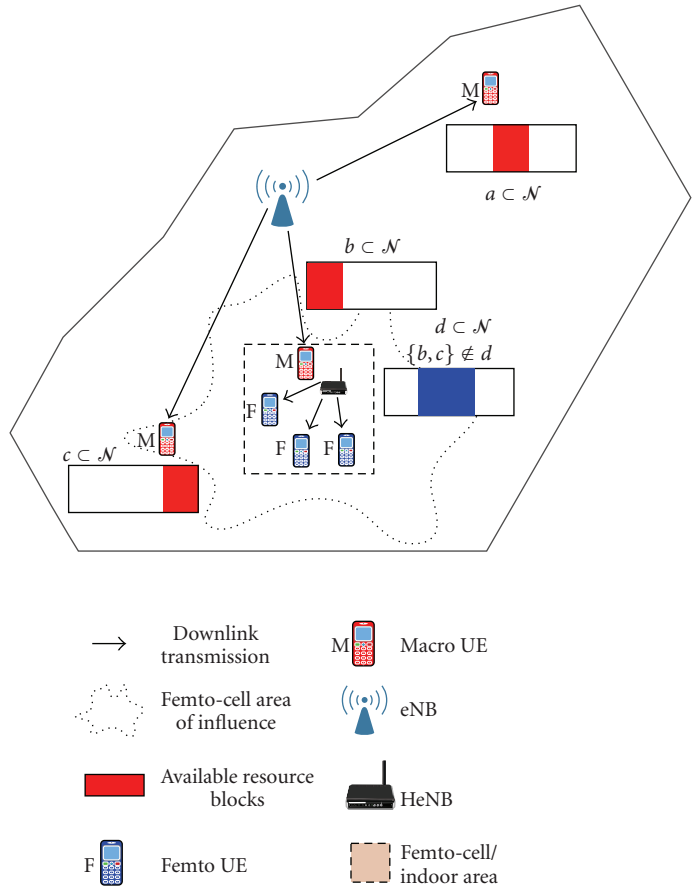

FIGURE 1: Resource partitioning in the vicinity of a femto-cell. The femto-cell is forbidden from using downlink resources allocated to nearby macro UEs, that is, b and c, but may continue using the set of resources a.

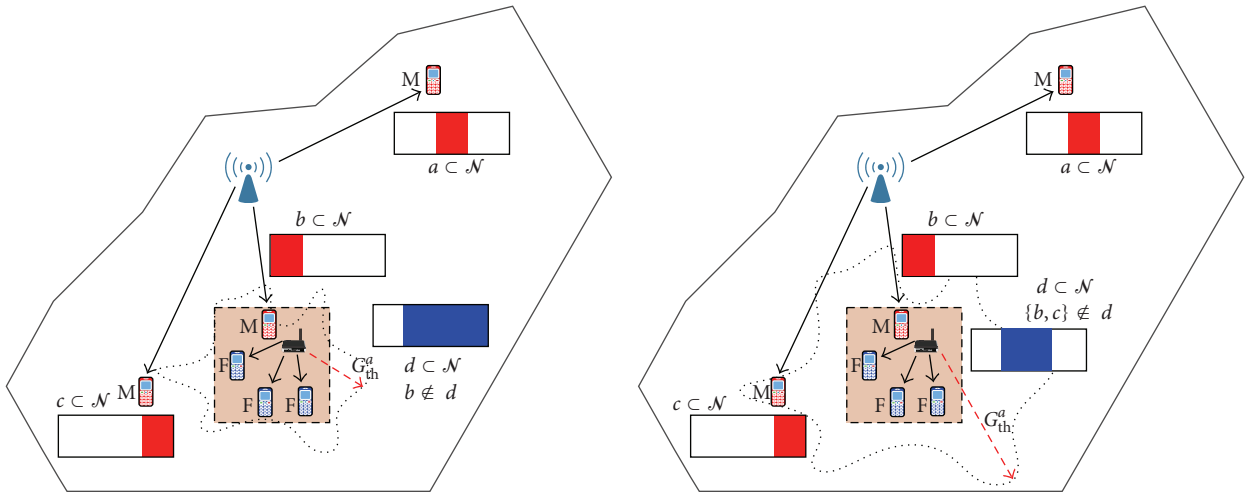

(a) High interference threshold

(b) Low interference threshold

FIGURE 2: Resource partitioning with two different thresholds ($G^a_{\text{th}} > G^b_{\text{th}}$). Using a lower threshold b leads to a larger number of partitioned resources.

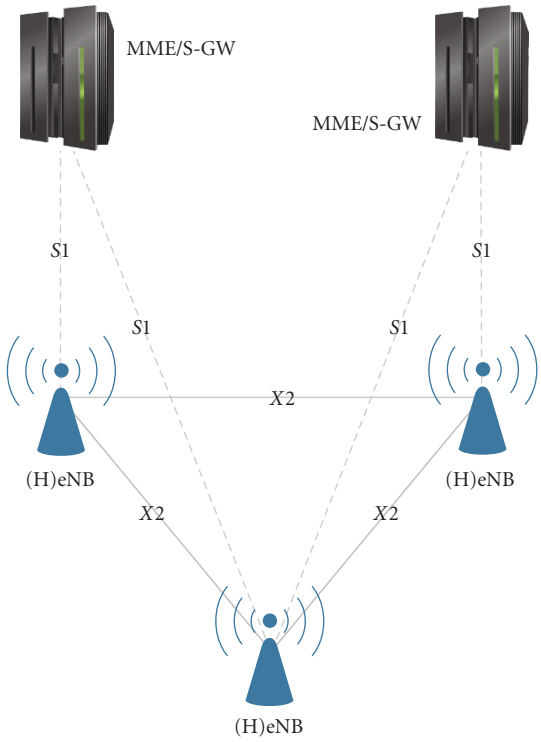

Figure 3: Overall LTE architecture showing S1 and X2 interfaces.

contains the cell-IDs, a UE can establish a list of neighboring eNBs. Knowledge of the cell-ID also enables UEs to read the cell-specific reference signals (also known as training symbols or pilots) of neighboring eNBs, that are needed to carry out RSRP measurements. These enable the estimation of the average channel gain between the UE and the surrounding eNBs, $\overline{G}^{u,v}$, in (10). RSRP for a specific cell is defined as the linear average over the power contributions (in W) of the Resource Elements (REs) which carry cell-specific reference signals within the considered measurement frequency bandwidth [11]. As HeNBs also broadcast their cell-ID in the BCH, as well as cell-specific reference signals, RSRP measurements allow the identification of HeNBs that are in close proximity of a macro UE. We note that this does not introduce any additional overhead because we utilize an existing signaling procedure between macro UEs and eNBs.

The eNB needs to inform the HeNB that causes interference of the restricted resources $\overline{\mathcal{N}_i}$ it must not use according to (11). This involves defining the transport of control information from eNBs to HeNBs using the LTE network architecture shown in Figure 3. The S1 interface connects the Serving Gateway (S-GW)/Mobility Management Entity (MME) with a pool of neighboring eNBs. The MME is a control node that processes the signaling between the UE and the core network (CN). Neighboring eNBs are interconnected via the X2 interface, that conveys control information related to handover and interference coordination. The X2 interface is therefore particularly suited for signaling related to femto-to-macro interference avoidance [16, 17].

In LTE, the network architecture is flat such that when a UE is handed over, to improve latency and efficiency, the handover procedure is exclusively controlled by the source and destination eNBs [25]. For intra-LTE handover, the default procedure is that the source eNB buffers the data and passes it to the destination eNB over the X2 interface. If no X2 connection exists between the source and destination eNBs, the handover is performed over the S1 interface. However, from the UE's viewpoint, there is no difference between the two types of handover [25]. In the case of closed-access femto-cells, where a handover is not possible between a source H/eNB and a destination HeNB, the proposed resource partitioning procedure requires that signaling information is conveyed from the source eNB to the destination HeNB.

In the LTE downlink, a bitmap known as the Relative Narrowband Transmit Power (RNTP) indicator is exchanged over the X2 interface between eNBs. The RNTP indicator is used by an eNB to signal to neighboring eNB on which RBs it intends to transmit with high power in the near future. Each bit of the RNTP indicator corresponds to one RB in the frequency domain and is used to inform the neighboring eNBs if the eNB in question is planning to exceed the transmit power for that RB or not [26]. The value of the threshold and the time period for which the indicator is valid are configurable parameters. This bitmap is intended to enable neighboring cells to estimate the amount of interference on each RB in future frames and therefore schedule their UEs accordingly. Furthermore, the source and destination cell IDs need is contained in the RNTP.

The DL-HII messages that indicate which resources a particular HeNB must not use may be conveyed by a bitmap that is equivalent to that of the RNTP indicator. Provided that HeNBs are also connected to the X2 interface, DL-HII messages emitted by eNBs may be configured to perform resource partitioning at certain HeNBs by using the format of the RNTP indicator. Suppose that macro UE u served by eNB v_u is trapped within the coverage area of a closed-access femto-cell, served by HeNB i. Then resource partitioning is implemented by sending a DL-HII message to HeNB i, where ones and zeros correspond to RBs where HeNB i may and may not transmit, respectively. The transmission format of the RNTP indicator is therefore perfectly suited for DL-HII messages.

In order to avoid that DL-HII messages are to be sent every subframe (i.e., at 1 ms intervals), the *lifetime* of DL-HII messages could be configured in a dedicated field within the DL-HII message format. Dependent on the underlying service the macro UE is using, the eNB estimates for how long the RBs utilized macro UE are to be reserved, and notes this estimate as the lifetime of the DL-HII message. Unless DL-HII message is updated before its lifetime expires, the HeNB may then reuse the restricted RBs after the lifetime of the DL-HII message has expired. This limits the signaling overhead due to DL-HII messages to a level comparable to that of a handover procedure, which is needed, for example, for macro-to-femto-cell handover in open access systems.

Historical UE information is propagated between eNBs during the X2 handover procedure [25]. Historical UE

information consists of the last few cells visited by the UE, together with the time for which the UE was camped at that eNB. The historical information is used to determine the occurrence of a handover ping-pong between cells. This is also a source of information that is useful in the context of resource partitioning. If a UE is camped to the last few eNBs for a short time interval, the resource partitioning procedure need not be carried out. This can be done to avoid unnecessary signaling.

4. System Level Simulation Setup

4.1. User Distribution and Sectorized eNBs. The simulation area comprises a two-tier, tessellated hexagonal cell distribution. In order to eliminate edge effects with regards to interference, additional two tiers are simulated. However, statistics are taken only from the central two tiers. The eNBs are placed at the junction of three hexagonal cells, such that each cell can be considered as a sector. In this way, each eNB serves three sectors, with each sector reusing all frequency resources. For each sector, the azimuth antenna pattern, $A(\theta)$, is described by [24]

$$A(\theta) = -\min\left[12\left(\frac{\theta}{\theta_{3\text{dB}}}\right)^2, A_m\right], \tag{12}$$

where the $\theta_{3\text{dB}} = 70^\circ$ is the angle from the central lobe at which the gain reduces to half the maximum value and $A_m = 20\,\text{dB}$ is the maximum possible attenuation due to sectorization.

We follow the simulation assumptions described in [24] where a 5×5 grid model is used to simulate femto-cell deployment. This setup models a single-floor building with 25 apartments that are arranged in a 5×5 grid. An HeNB may exist in an apartment with probability p_1. Furthermore, an HeNB may be active with probability p_2. Therefore, the probability p that an apartment contains an active HeNB is given by $p = p_1 p_2$. Every apartment that contains an active HeNB contains exactly one associated femto UE. These are dropped randomly and uniformly within the apartment with a specified minimum separation from the HeNB. In addition to this, macro UEs are also randomly and uniformly dropped within the tiered hexagonal system. As a result, it is possible that a macro UE lies within the confines of an apartment. Figure 4 shows one instance of a distribution of four apartment blocks and ten macro UEs per macro sector. It is observed that some macro UEs lie within apartment blocks. We assume a closed-access policy so that such macro UEs, despite their indoor location, are served by the eNB. In such a situation, these macro UEs suffer from severe interference originating from the nearby HeNBs. Macro UEs lying either inside an apartment block containing active HeNBs or very close to such an apartment block are the likely victims of high downlink femto-to-macro interference. The concept of resource partitioning addresses the mitigation of interference experienced by such macro UEs in the downlink. The macro UEs indicated by arrows in Figure 4 are the potential recipients of high interference originating from nearby femto-cells.

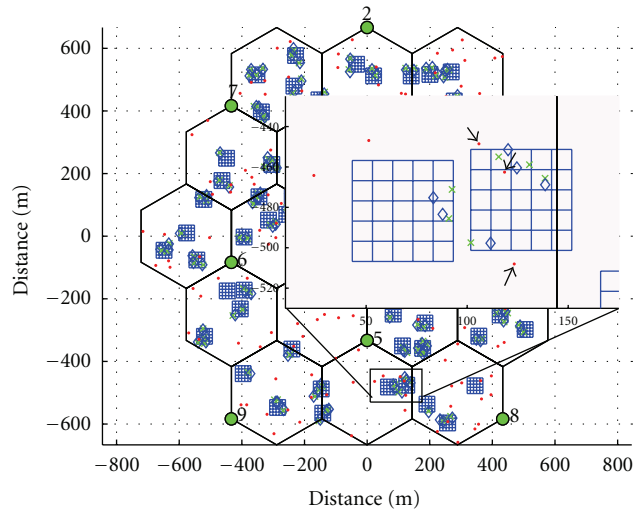

Figure 4: Four apartment blocks and ten macro UEs per macro sector. Macro UEs are denoted by red dots, femto UEs by blue diamonds, HeNBs by green crosses and eNBs by filled green circles, each denoted with a number. The close-up shows a few marked macro UEs undergoing potentially severe downlink interference from nearby active femto-cells.

In this particular case, if one or more HeNBs are indeed the cause of high interference, they will partition resources so as to enable the vulnerable macro UEs to attain a satisfactory downlink SINR.

4.2. Time Evolution. Since the resource allocation is random in nature, each run of the Monte Carlo simulation is iterated over a series of snapshots to obtain statistically accurate results. The duration of a snapshot is equivalent to the duration of one LTE subframe and the run is allowed to iterate over ten subframes (one LTE frame). At each iteration, the allocation of resources is randomized. It is assumed that the UEs are quasistatic for the duration of the run.

5. Results

The simulation is run for a full-buffer traffic model, that resembles the worst case scenario where all users in the system are active simultaneously. Furthermore, the users in the system are assumed to be static for the duration of the snapshot, so that the effects due to Doppler spread are neglected. Perfect synchronization in time and frequency is assumed, such that interference between neighboring RBs can be neglected as well. Relevant parameters used for the simulation are shown in Table 3.

Clearly, more than one macro UE can be affected by the same apartment block and more than one apartment block can affect the same macro UE (as demonstrated in Figure 4). The offending HeNBs must then perform resource partitioning using the method described in Sections 3.2 and 3.3. Due to the effects of shadowing, the corresponding exclusion region is not a circular area.

Table 3: Simulation parameters.

Parameter	Value
Avg. 5×5 apartment blocks per macro-cell sector	$\{4, 14\}$
Avg. macro UEs per macro-cell sector	10
Inter-site distance	500 m
Individual apartment dimensions	$10 \times 10\ \text{m}^2$
HeNB deployment probability, p_1	0.2
HeNB activation probability, p_2	0.5
Femto UEs per active femto-cell	1
Downlink FDD band	[2.62, 2.63] GHz
Tot. number of available RBs, N	50
RB bandwidth, B_{RB}	180 kHz
Thermal noise, η	-174 dBm/Hz
eNB transmit power per RB per sector, P_{m}	29 dBm
HeNB transmit power per RB, P_{f}	3 dBm
eNB antenna gain	14 dBi
Sectors per eNB	3
Min. distance between macro UE and eNB	35 m
Min. distance between femto UE and HeNB	0.2 m
Number of macro/femto UE Rx antennas	2 Rx
Wall penetration loss, L_{W}	20 dB
Interference threshold, I_{th}	$\{-72, -87\}$ dBm
Subframe time duration, t_{s}	1 ms

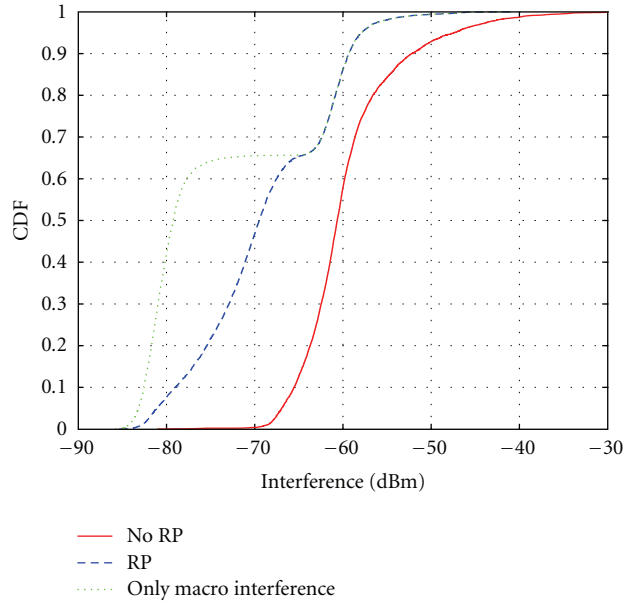

Figure 5: CDFs showing downlink interference for affected macro UEs in systems with and without resource partitioning, compared against a system with no femto interference.

For a meaningful performance assessment, the definition of "affected" macro and femto UEs is to be introduced. A macro UE is said to be "affected" if its average channel gain to at least one HeNB exceeds the predefined threshold I_{th}, as defined in (10). This section shows results for different classes of UEs: overall macro (all macro UEs in the system, regardless of their location), overall femto (all femto UEs, all lying strictly indoors associated with an active HeNB), affected macro (only macro UEs in the vicinity of active femto-cells as described above), and affected femto (only femto UEs served by offending HeNBs).

Figure 5 demonstrates the need for femto-to-macro interference coordination and the benefit of resource partitioning. The cumulative distribution function (CDF) of downlink interference for affected macro UEs with and without resource partitioning is shown in this figure. An interference threshold of $I_{\text{th}} = -72$ dBm is used, which translates to $G_{\text{th}} = -75$ dB. For comparison purposes, a third CDF is displayed showing the interference only from the macro layer, where HeNB transmit powers are reduced to zero, keeping the allocation of resources unchanged. This third case represents the "ideal" situation without interference from the femto layer. This "ideal" case therefore represents an upper bound for the performance of any femto-to-macro interference avoidance scheme. It is clear from the figure that resource partitioning reduces the interference by approximately 10 dB at the 50th percentile. Furthermore, it is seen that resource partitioning approaches the performance of the upper bound particularly in the high interference regime, where the offending HeNBs suppress transmission on the vulnerable RBs. The difference between the lower interference regimes of the curve with resource partitioning and the case without femto interference indicates the amount of additional interference caused by those HeNBs that do not perform resource partitioning, because they do not lie in the vicinity of any vulnerable macro UEs. It is clear from this figure that there is a significant benefit from resource partitioning. The following figures show the effect of resource partitioning on the macro and femto performance.

The capacities of combined macro and femto-cell depicted in Figures 6 through 9 are compared against a benchmark system that emulates a state-of-the-art cellular network. In this benchmark system, no HeNBs exist, and all UEs previously classified as femto UEs are served by the outdoor eNBs. *All* UEs in the benchmark system are therefore macro UE and must therefore share the available macro resources.

Figure 6 shows the overall downlink macro user capacity for 4 and 14 grids with 10 macro UEs per macro-cell sector with the interference thresholds $I_{\text{th}} = -72$ and -87 dBm. The two I_{th} thresholds are chosen because they represent two extreme cases: one in which the exclusion region causes approximately 13% of HeNBs to partition resources ($I_{\text{th}} = -72$ dBm) and the other (-87 dBm) where the exclusion region causes approximately 76% of HeNBs to partition resources. In this case, capacity statistics are collected from all macro UEs, regardless of whether they lie outdoors or indoors and regardless of whether they are vulnerable to heavy HeNB interference or not. It is observed that when resource partitioning is applied, a consistent gain is achieved over the benchmark, where, both macro and femto-cells fully utilise all available resources.

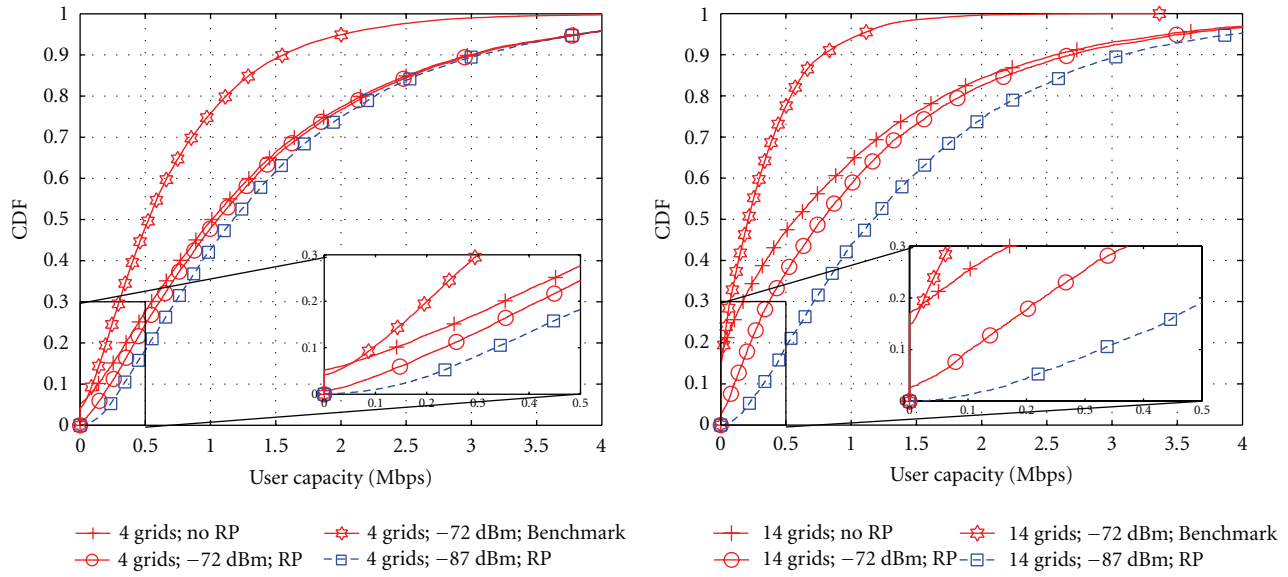

(a) 4 5 × 5 grids per macro-cell sector

(b) 14 5 × 5 grids per macro-cell sector

Figure 6: CDFs of the overall downlink macro user capacity for a system with and without resource partitioning, compared against the benchmark system with no femto-cell deployment.

Figure 6 reveals that there is a higher resource partitioning gain in the lower capacity regime (lower percentiles of the CDF). This is due to affected macro UEs that severely suffer from interference originating from nearby HeNBs. In the higher capacity regime, resource partitioning gains diminish because macro UEs achieving high capacities typically lie outdoors, well protected from interfering HeNBs through walls, so that the dominant interference for such macro UEs originates from other eNBs.

It is observed that the user capacity of the system with 14 grids per macro-cell sector shown in Figure 6(b) is consistently worse than the performance of the system with lower grid density shown in Figure 6(a). This is expected as increasing the grid density increases the amount of interference originating from the femto layer. For the benchmark, a higher grid density means that the same amount of resources in the macro-cell have to be shared among a higher number of users, thus compromising user capacity. Interestingly, it is observed that when $I_{\text{th}} = -87$ dBm, the performance of the systems with either grid density are almost identical. This is attributed to the fact that in either case, the number of macro UEs remains the same, and the high value of I_{th} then ensures that the majority of HeNBs partition resources. As a result, the amount of femto interference stays largely independent of the grid density. Of note is that a decreasing I_{th} enhances the attainable gains in macro UE capacity.

It is clear from Figure 6 that augmenting a cellular network with femto-cell deployment yields tremendous capacity gains over the benchmark system. These gains are attributed to two reasons. First, in the benchmark system, all former femto UEs are served by the outdoor eNB, where high wall penetration losses result in a highly attenuated signal. The second reason is that in the benchmark system, all UEs must share the macro resources, so that each UE is assigned fewer RBs compared to the case with femto-cell deployment. For four apartment blocks per sector (Figure 6(a)), with each apartment having a 10% probability of containing an active HeNB, each sector contains, on average, ten femto UEs in addition to the ten macro UEs. This means that in the benchmark system, each macro UE is allocated half the number of RBs in comparison to the system with femto-cell deployment. The situation is obviously worsened in the 14 grid per sector case, as shown in Figure 6(b). This is also responsible for the benchmark system showing the highest outage. In this context, a UE goes into outage if the achieved SINR on all RBs is less than γ_{min}.

Finally, in the very low capacity regime (<0.1 Mbps in either case), the benchmark system outperforms the system without resource partitioning. This is due to excessive femto-to-macro interference experienced by macro UEs trapped within the coverage area of femto-cells.

Figure 7 shows the overall femto user capacity on the downlink. Results are gathered for all femto UEs, regardless of whether they are in the vicinity of a vulnerable macro UE. In general, very high capacities are achieved in femto-cells. This is due to the very short transmission distances within femto-cells, as well as outdoor interference protection through high wall penetration losses. We observe that in all cases, user capacities saturate at 39.6 Mbps, due to the upper bound of the link-to-system mapping (4). According to (4), the maximum achievable spectral efficiency is capped at $\overline{C}_{\text{max}} = 4.4$ bit/s/Hz, and because HeNBs only serve one femto UE, with all available resources $\mathcal{N}$ being allocated to this UE, this equates to a maximum downlink capacity of 39.6 Mbps.

Figure 7 also reveals that femto-cells must sacrifice some capacity when resource partitioning is in place. This is obvious because the affected HeNBs are forbidden from

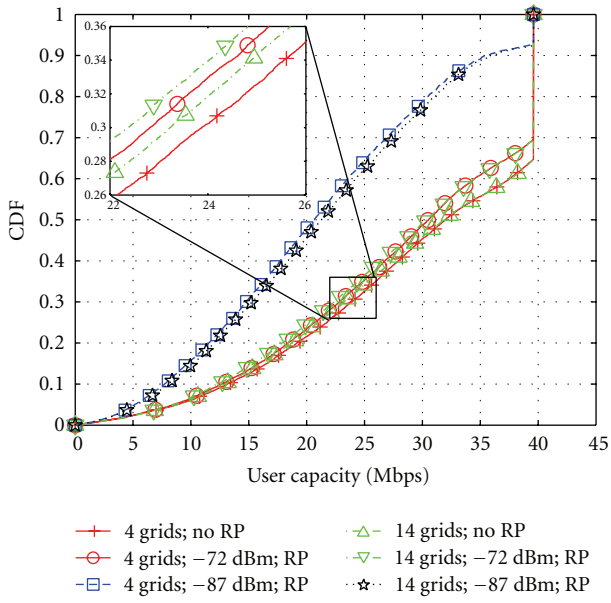

Figure 7: CDFs showing femto downlink user capacity for a system with resource partitioning compared against a system without resource partitioning.

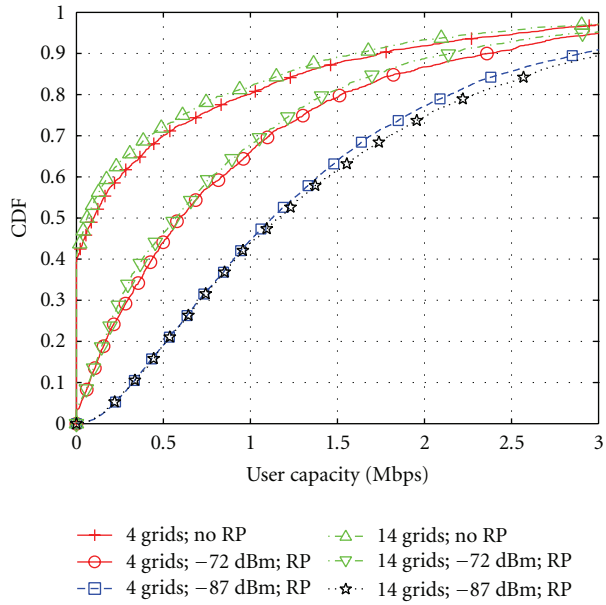

Figure 8: CDFs showing downlink user capacity only for affected macro UEs for a system with resource partitioning compared against a system without resource partitioning.

using RBs allocated to nearby macro UEs. Moreover, the lower the threshold I_{th} the higher the partitioning of femto-cell resources, and thus the lower the proportion of femto UEs that approach the maximum capacity. For $I_{\text{th}} = -72$ dBm, the degradation in femto user capacity is in the order of 1 Mbps. On the other hand, when $I_{\text{th}} = -87$ dBm, the degradation increases to approximately 10 Mbps. It is important to note that owing to the full buffer assumption, the degradation in femto user capacities reflects a worst case scenario. In case femto-cells are not assigned all available resources, the degradation due to resource partitioning is obviously lower.

A trade-off between the improvement in macro capacity and degradation of femto capacity exists. Optimization of this trade-off depends on the acceptable degradation of macro-cell capacity (see Figure 6), in particular at the low percentiles of the corresponding CDF. This enables the determination of the appropriate threshold I_{th}, which in turn results in a certain degradation of femto-cell performance.

Figures 8 and 9 concentrate on affected macro and femto UEs. Figure 8 shows the capacity performance of affected macro UEs. It is observed that resource partitioning delivers a significant gain to the downlink performance of affected macro UEs. It is seen that regardless of the grid density, with $I_{\text{th}} = -72$ and -87 dBm, a five and, respectively, tenfold capacity increase of affected macro UEs is observed.

Figure 9 shows that the sacrifice in downlink capacity that affected femto UEs incur due to resource partitioning. It is observed that UEs associated with HeNBs that must partition resources incur a reduction in capacity of approximately 25% with $I_{\text{th}} = -72$ dBm and 39% with $I_{\text{th}} = -87$ dBm. It is important to note that for a sacrifice of 39% of femto capacity, the affected macro UEs are rewarded with a tenfold

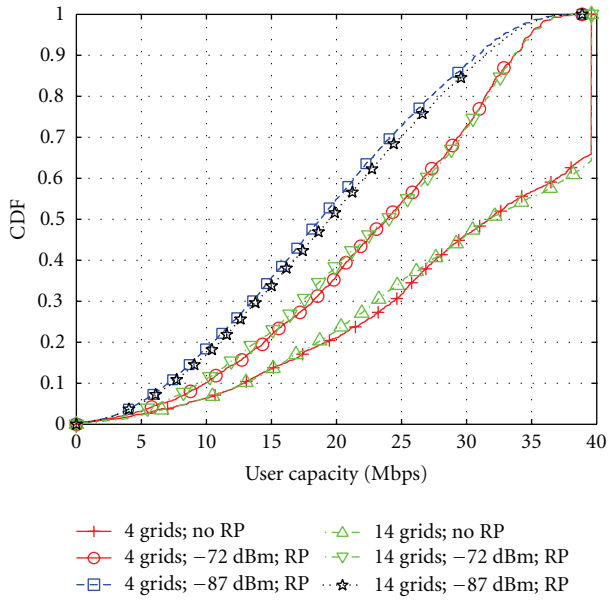

Figure 9: CDF showing downlink user capacity only for affected femto UE for a system with resource partitioning compared against a system without resource partitioning.

capacity increase. We note that with either grid density, the affected macro and femto UE performance is almost identical because in both cases, the macro UE density remains the same and therefore, every HeNB must partition the same proportion of resources.

The sum system capacity in the downlink normalized per macro sector shows some interesting trends. With

Table 4: Femto UE capacity degradation and macro UE capacity improvement.

I_{th} value	Overall femto UE degradation	Affected macro UE improvement	Affected femto UE degradation
−72 dBm	1 Mbps	5x	25%
−87 dBm	10 Mbps	10x	39%

a grid density of 4 grids per macro-cell sector and $I_{th} = -72$ dBm, the use of resource partitioning results in an affected macro UE capacity increase of 6.4% at the cost of a 2.8% degradation in femto capacity. However, when $I_{th} = -87$ dBm, a 14.2% increase in macro capacity is accompanied by a 29.6% decrease in femto capacity. The situation is different for the case when the grid density is increased to 14 grids per macro sector. When $I_{th} = -72$ dBm, a 15.7% increase in macro capacity is attained at a the expense of a 2.8% decrease in femto capacity. For $I_{th} = -87$ dBm, resource partitioning results in a 53.2% increase in affected macro UE capacity with a 25.1% decrease in femto capacity. This shows that with decreasing grid densities, a relatively high interference threshold I_{th} becomes more effective.

For convenience, the femto UE degradation and macro UE improvement in capacity through the use of resource partitioning are listed in Table 4.

6. Summary and Conclusion

Femto-cell deployment poses a viable complement to cellular networks. Operators need to bear low cost in their deployment because they are installed directly by the users themselves. Furthermore, because they share both, the radio access scheme and the frequency band with eNBs, they are compatible with legacy UEs. Aside from these benefits, a cellular network stands to significantly gain in overall system throughput through the widespread deployment of HeNBs. Not only do HeNBs improve indoor coverage, bringing broadband-like experience directly to the handset, but they also offload resources from the eNB that can be utilized to improve coverage to outdoor users.

It has been seen that in a closed-access system, macro UEs lying in the proximity of femto-cells experience at least as much downlink interference from HeNBs as they do from eNBs. It has been demonstrated that by introducing LTE-specific resource partitioning, the capacity of such macro UEs can be boosted by a factor of ten. The cost incurred by femto UE in doing so is minimal as they lose less than half of their capacity (which is more than one order of magnitude higher than macro UE downlink capacity). Users therefore experience a very high throughput inside femto-cells due to the favorable channel conditions and continue to do so even in the presence of resource partitioning. Introducing resource partitioning to a closed-access system with femto-cell deployment substantially boosts the sum system capacity while ensuring reliable macro-cell operation.

Acknowledgments

Initial parts of this work were supported by **DFG Grant** HA 3570/2-1 as part of program SPP-1163 (adaptability in heterogeneous communication networks with wireless access—AKOM) while some latter parts of this work have been performed within the framework of the CELTIC project CP5-026 WINNER+. Harald Haas acknowledges the Scottish Funding Council support of his position within the Edinburgh Research Partnership in Engineering and Mathematics between the University of Edinburgh and Heriot Watt University.

References

[1] M.-S. Alouini and A. J. Goldsmith, "Area spectral efficiency of cellular mobile radio systems," *IEEE Transactions on Vehicular Technology*, vol. 48, no. 4, pp. 1047–1066, 1999.

[2] T. Nihtilä, "Increasing femto cell throughput with HSDPA using higher order modulation," in *Proceedings of the IEEE International Networking and Communications Conference (INCC '08)*, pp. 49–53, Lahore, Pakistan, May 2008.

[3] V. Chandrasekhar, J. G. Andrews, and A. Gatherer, "Femtocell networks: a survey," *IEEE Communications Magazine*, vol. 46, no. 9, pp. 59–67, 2008.

[4] Z. Bharucha, I. Ćosović, H. Haas, and G. Auer, "Throughput enhancement through femto-cell deployment," in *Proceedings of the 7th IEEE International Workshop on Multi-Carrier Systems & Solutions (MC-SS '09)*, pp. 311–319, Herrsching, Germany, May 2009.

[5] Z. Bharucha, H. Haas, A. Saul, and G. Auer, "Throughput enhancement through femto-cell deployment," *European Transactions on Telecommunications*, vol. 21, no. 4, 2010.

[6] M. Etoh, T. Ohya, and Y. Nakayama, "Energy consumption issues on mobile network systems," in *Proceedings of the International Symposium on Applications and the Internet (SAINT '08)*, pp. 365–368, IEEE, Turku, Finland, July-August 2008.

[7] H. Haas and G. J. R. Povey, "Capacity analysis of a TDD underlay applicable for UMTS," in *Proceedings of the 10th IEEE International Symposium on Personal, Indoor and Mobile Radio Communications (PIMRC '99)*, p. A6-4, Osaka, Japan, September 1999.

[8] H. Haas and G. J. R. Povey, "A capacity investigation on UTRA-TDD utilising underused UTRA-FDD uplink resources," in *Proceedings of the IEE Colloquium on UMTS Terminals and Software Radio*, pp. 1–7, Glasgow, Scotland, April 1999, Ref. no. 1999/055.

[9] P. K. Jain, H. Haas, and S. McLaughlin, "Capacity enhancement using ad hoc pico-cells and TDD underlay," in *Proceedings of the 17th IEEE International Symposium on Personal, Indoor and Mobile Radio Communications (PIMRC '06)*, pp. 1–5, Helsinki, Finland, September 2006.

[10] X. Yang, G. Feng, and C. K. Siew, "Call admission control for multi-service mobile networks with bandwidth asymmetry between uplink and downlink," in *Proceedings of the IEEE Global Telecommunications Conference (GLOBECOM '04)*, vol. 5, pp. 3285–3289, November-December 2004.

[11] 3GPP, "Physical Channels and Modulation (Release 8)," 3GPP TS 36.211 V 8.2.0, March 2008, http://www.3gpp.org/ftp/Specs.

[12] D. López-Pérez, A. Valcarce, G. De La Roche, and J. Zhang, "OFDMA femtocells: a roadmap on interference avoidance,"

IEEE Communications Magazine, vol. 47, no. 9, pp. 41–48, 2009.

[13] H. Claussen, "Performance of macro- and co-channel femtocells in a hierarchical cell structure," in *Proceedings of the 18th IEEE International Symposium on Personal, Indoor and Mobile Radio Communications (PIMRC '07)*, pp. 1–5, Athens, Greece, September 2007.

[14] L. T. W. Ho and H. Claussen, "Effects of user-deployed, co-channel femtocells on the call drop probability in a residential scenario," in *Proceedings of the 18th IEEE International Symposium on Personal, Indoor and Mobile Radio Communications (PIMRC '07)*, pp. 1–5, Athens, Greece, September 2007.

[15] V. Chandrasekhar and J. Andrews, "Uplink capacity and interference avoidance for two-tier femtocell networks," *IEEE Transactions on Wireless Communications*, vol. 8, no. 7, pp. 3498–3509, 2009.

[16] 3GPP, "X2 General Aspects and Principles (Release 8)," 3GPP TS 36.420 V8.0.0, December 2007, http://www.3gpp.org/ftp/Specs.

[17] 3GPP, "X2 Application Protocol (X2AP) (Release 8)," 3GPP TS 36.423 V8.2.0, June 2008, http://www.3gpp.org/ftp/Specs.

[18] T. S. Rappaport, *Wireless Communications: Principles and Practice*, Prentice Hall, Upper Saddle River, NJ, USA, 2nd edition, 2001.

[19] 3GPP, "Evolved Universal Terrestrial Radio Access (E-UTRA); Radio Frequency (RF) System Scenarios," 3GPP TR 36.942 V 8.2.0, May 2009, http://www.3gpp.org/ftp/Specs.

[20] A. Persson, T. Ottosson, A. Saul, G. Auer, and M. Afgani, "On the performance of inter-sector scheduling in OFDMA systems," in *Proceedings of the 11th International OFDM Workshop (InOWo '06)*, Hamburg, Germany, August 2006.

[21] ITU-R Working Party 5D (WP5D)—IMT Systems, "Report of correspondence group for IMT.EVAL," Tech. Rep. 124, Dubai, United Arab Emirates, May 2008.

[22] W. Wang, T. Ottosson, M. Sternad, A. Ahlén, and A. Svensson, "Impact of multiuser diversity and channel variability on adaptive OFDM," in *Proceedings of the 58th IEEE Vehicular Technology Conference (VTC '03)*, pp. 547–551, Orlando, Fla, USA, October 2003.

[23] NTT DOCOMO, "New Evaluation Models (Micro Cell, Indoor, Rural/High-Speed)," 3GPP TSG RAN WG1 R1-082713, July 2008, http://www.3gpp.org/ftp/tsg_ran/WG1_RL1/TSGR1_53b/Docs.

[24] 3GPP, "Simulation Assumptions and Parameters for FDD HeNB RF Requirements," 3GPP TSG RAN WG4 R4-092042, May 2008, http://www.3gpp.org/ftp/Specs.

[25] S. Sesia, I. Toufik, and M. Baker, Eds., *LTE—The UMTS Long Term Evolution: From Theory to Practice*, John Wiley & Sons, New York, NY, USA, 1st edition, 2009.

[26] 3GPP, "Evolved Universal Terrestrial Radio Access (E-UTRA); Physical Layer Procedures (Release 8)," 3GPP TS 36.213 V 8.8.0, September 2009, http://www.3gpp.org/ftp/Specs.